frontiers | Frontiers in Physics

TYPE Review
PUBLISHED 07 October 2022
DOI 10.3389/fphy.2022.969129

OPEN ACCESS

EDITED BY
Xuzong Chen,
Peking University, China

REVIEWED BY
Wang Qing,
Peking University, China
Xiong Wei,
Peking University, China

*CORRESPONDENCE
Lin Li,
lilin18800179956@buaa.edu.cn
Ying Liu,
liu_ying@buaa.edu.cn

SPECIALTY SECTION
This article was submitted to Atomic and Molecular Physics,
a section of the journal
Frontiers in Physics

RECEIVED 14 June 2022
ACCEPTED 20 September 2022
PUBLISHED 07 October 2022

CITATION
Zhai Y, Yue Z, Li L and Liu Y (2022), Progress and applications of quantum precision measurement based on SERF effect.
Front. Phys. 10:969129.
doi: 10.3389/fphy.2022.969129

Progress and applications of quantum precision measurement based on SERF effect

Yueyang Zhai[1,2], Ziqian Yue[1], Lin Li[1]* and Ying Liu[1,2]*

[1]Key Laboratory of Ultra-Weak Magnetic Field Measurement Technology, Ministry of Education, School of Instrumentation and Optoelectronic Engineering, Beihang University, Beijing, China, [2]Beihang Hangzhou Innovation Institute Yuhang, Hangzhou, China

With the development of quantum precision measurement technology, measurement methods based on magnetic, optical and atomic interactions have started to receive widespread attention. Among them, quantum precision measurement based on the spin-exchange relaxation-free (SERF) effect shows great potential by its ultra-high measurement sensitivity. This paper introduces the basic operation principles of the magnetic field and inertia measurement based on the SERF effect, and focuses on the research progress and applications of SERF quantum precision measurement in fundamental physics, inertial navigation and biomedicine. Finally, we propose a prospect for the directions of SERF quantum precision measurement.

KEYWORDS

SERF, magnetic field measuremenet, inertia measurement, fundamental physics, inertial navigation, biomedicine

Introduction

Physical quantity information plays a significant role in precise measurement. With the development of multi-disciplinary, multi-technology and multi-Frontier scientific exploration, such as quantum optics, atomic manipulation technology, atomic physics, optics, material science and microelectronics, a door has been opened for precision measurement. Precision measurement has experienced the development of electromechanical and photoelectric methods, and now it has entered the quantum era [1, 2]. Quantum precision measurement based on the cold and hot atoms can realize high precision and high sensitivity measurement of physical quantities [3–5]. Through the research and technical application of high-precision and high-sensitivity measurement methods, quantum level limit detection, precise operation and comprehensive application can be realized. With the discovery of new physical effects, new control principles and methods in the field of quantum manipulation, the sensitivity of quantum precision measurement has increased by an order of magnitude [6]. At present, the seven basic physical quantities that represent the highest level of precision measurement have all been quantized. In addition to the seven basic physical quantities, extremely weak magnetic field measurement and inertial measurement are also moving towards the quantum era [7, 8].

Quantum precision magnetic field measurement is of great value in the fields of electric dipole moment (EDM) measurement in Frontier physics research [5], brain magnetic and cardiac magnetic field measurement in brain science and medicine [9, 10], deep space magnetic field exploration in space science [11], *etc.* Quantum inertial measurement has broad application prospects in Frontier physics research such as Charge conjugation-Parity transformation-Time reversal (CPT) conservation [12, 13] and long-time high-precision navigation of moving vehicles [14].

The spin effect based on spin-exchange relaxation-free (SERF) developed in the early 21st century can realize extremely weak magnetic field measurement [7] and ultra-high sensitivity inertial measurement [8]. The theoretical sensitivity of the extremely weak magnetic field measurement based on SERF effect can reach the order of aT (10^{-18} T), which represents the new development direction of the world's precision extremely weak magnetic field measurement technology. Based on SERF effect, an ultra-high sensitivity inertial measurement with a theoretical accuracy of $10^{-12°}$/s/$Hz^{1/2}$ can be achieved, which is four orders of magnitude higher than the highest international index. There is no doubt that the research of quantum precision measurement based on SERF effect will play an important role in a wide range of applications.

In this paper, we review the development and application of quantum precision measurement technology based on SERF effect. More specifically, we describe the principle of atomic SERF effect, and review the progress and application of SERF effect in fundamental physics, inertial navigation and biomedicine. Finally, we propose a prospect for quantum precision measurement technology based on SERF effect.

Fundamental principles

Spin is an endogenous property of atoms. Atomic spins include electron spin and nuclear spin, which have angular momentum and magnetic moment, respectively. Since the atomic spin is sensitive to the magnetic field or rotation relative to the inertial space, the measurement of magnetic field or inertial rotation can be achieved by detecting the spin precession of atoms [15, 16]. The process of measurement is roughly divided into the following three stages: 1. polarization of spin; 2. interaction of spin with external physical fields; 3. measurement of spin polarization [17]. Atomic spin polarization is the basis for measuring atomic spin precession. The spins of atoms in their natural states are haphazard, and an applied magnetic field and pumped light can give their haphazard spins a macroscopic pointing, which is called polarization [15]. However, while polarizing, a spin-exchange relaxation process is caused by spin-exchange collisions between atoms. The spin relaxation process indicates spin depolarization, reducing the measurement's performance.

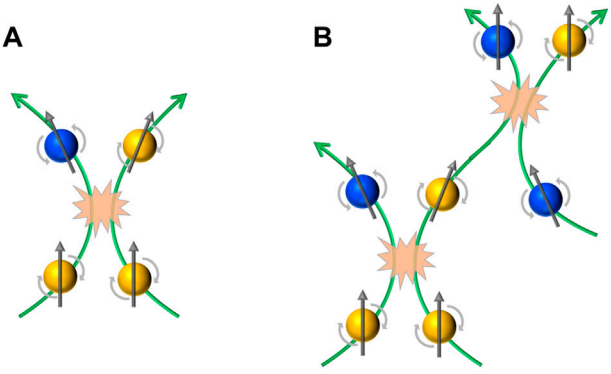

FIGURE 1
Spin-exchange collisions **(A)** Spin-exchange relaxation; **(B)** Spin-exchange relaxation-free [7].

Happer et al. found that if the atomic density is increased and the atoms are placed in a weak magnetic field, the spin-exchange rate of the atoms can be much larger than the atomic Larmor precession frequency [18], at which point the relaxation due to spin exchange collisions is greatly reduced and disappears completely under zero magnetic field conditions. This physical phenomenon is called the atomic spin-exchange relaxation-free (SERF) regime [19], which is expressed as a return to the initial polarization regime before the polarized atom can depolarize [20]. It was found that the mechanism of the SERF regime is that the high atomic density substantially increases the spin-exchange rate between atoms, and the weak magnetic field significantly reduces the Larmor precession frequency of atoms, then the whole atomic system enters into a fast spin-exchange regime [7]. The atoms quickly traverse all the ground state hyperfine sublevels in a very short time and rapidly transition between hyperfine energy levels. Since the higher hyperfine energy levels have more sublevels, with the pumping light pumping, the atoms have a higher probability of settling to the higher hyperfine energy levels, and the total spin of the atomic system remains in the same direction [21]. Figure 1 shows the schematic diagram of atomic spin-exchange collisions. Therefore, in the SERF regime, all the atoms on the hyperfine energy levels are locked together to move coherently, and spin-exchange collisions no longer cause spin relaxation, which effectively reduces the total relaxation rate at high atomic number density conditions and substantially improves the measurement sensitivity.The SERF regime gives the atoms a consistent and stable spin-in motion. The property can be exploited for precision measurements of magnetic fields and inertial rotations. Since the first SERF magnetometer was developed in 2003 [7, 22], there is a rapid development in this research field in the past 2 decades. SERF atomic magnetometers use alkali metal atoms (K, Rb, Cs, *etc.*) as the atomic source, and

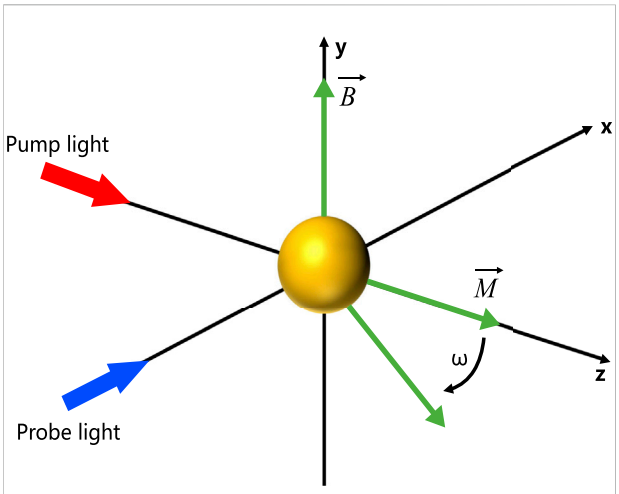

FIGURE 2
Schematic diagram of the operation principle of SERF atomic magnetometer. $\vec{B}$ is the external magnetic field. $\vec{M}$ represents the magnetic moment of the spin of alkali metal atom. ω is the frequency of the Larmor precession of magnetic moment. The pump light induces spin polarization of the alkali metal atoms. Under the action of the external magnetic field, the magnetic moment of the atomic spin will undergo Larmor precession, and another beam of probe light is irradiated perpendicular to the pump light to detect the Larmor precession [20].

the vapor cell generally includes alkali metal atoms, buffer gas (^{4}He), quenched gas (N_2), etc [23]. The general principle of the new magnetic field sensors is described as follows: a circularly polarized pump light is irradiated into the cell of alkali metal atoms, and the alkali metal atoms jump from the ground state to the excited state [24]. Then the alkali metal atoms reach the SERF regime. The external weak magnetic field brings a Larmor precession of the atomic spin. Another beam of linearly polarized light is applied to irradiate perpendicular to the pump light into the alkali metal cell for detecting the Larmor precession of the atomic spins [25]. The relationship exists between the external magnetic field and Larmor precession frequency is described as:

$$\omega = \gamma_e \|\vec{B}\|, \tag{1}$$

where ω represents the frequency of the Larmor precession; $\|\vec{B}\|$ is the norm of the external magnetic field intensity. And γ_e represents the electron spin-to-magnetic ratio of the alkali metal atom. The SERF atomic magnetometer measures the Larmor precession frequency of spin-polarized atoms in a magnetic field to indirectly obtain the magnitude of the magnetic field, thus achieving the magnetic field measurement [26]. Figure 2 displays the schematic diagram of the working principle of SERF atomic magnetometer. The theoretical sensitivity of the SERF atomic magnetometer is formulated as [7]:

$$\delta B = \frac{1}{\gamma_e \sqrt{nT_2Vt}}, \tag{2}$$

where n denotes the atomic number density; T_2 represents the transverse spin relaxation time; V is the sensitive volume of the alkali metal atom, and t is the measurement time.

The SERF inertial measurement was developed based on the measurement of magnetic fields using the SERF effect, and the first SERF effect-based inertial measurement device was proposed in 2005 [8], which has led to much research in this field. The SERF inertial measurement consists of SERF atomic magnetometer and hyperpolarized noble gas spin system synthesis. The schematic diagram of the operation principle of SERF inertial measurement is shown in Figure 3. The system integrates the electron spin of alkali metal atom and the nuclear spin of noble gas and carries out the angular velocity measurement by manipulating the electron spin of alkali metal atom to work in the SERF regime, and the nuclear spin of noble gas atom is strongly coupled with the electron spin of alkali metal atom. The general principle is described below.

The electron spin of the alkali metal atom has a fixed axis in the inertial space. In order to avoid the Larmor precession of this electron spin under the magnetic field, the coupled magnetometer structure is constructed by combining the nuclear spin of the noble gas and the atomic electron spin of the alkali metal. The electron spin of the alkali metal atom is strongly coupled to the nuclear spin of the noble gas in a specific case. Then the nuclear spin of the noble gas atom can automatically track and compensate for the change of the external magnetic field, thus isolating the influence of the magnetic field on the electron spin fixation of the alkali metal atom. When the carrier rotates, the electron spin direction of the alkali metal atom remains unchanged, while the detection laser is fixed on the carrier and rotates with the carrier, whose angle with the electron spin reflects the carrier's relative inertial space rotation. The nuclear spin of noble gas atoms is also fixed-axis in inertial space. When it compensates for the external magnetic field, a projection is produced in the direction of the angular velocity. The projection is related to the magnitude and direction of the angular velocity. The electron spin of the alkali metal atom will be affected by the projection of the nuclear spin, which will enhance the sensitivity of the detection laser to detect the electron spin pointing, and eventually improve the system's sensitivity to the angular velocity measurement [27]. The theoretical sensitivity of the SERF atomic spin inertia measurement is described as [13]:

$$\delta\Gamma = \frac{\gamma_n}{\gamma_e}\sqrt{\frac{1}{nVT_2t}}, \tag{3}$$

where γ_n is the nuclear spin-to-magnetic ratio of the noble gas atom.

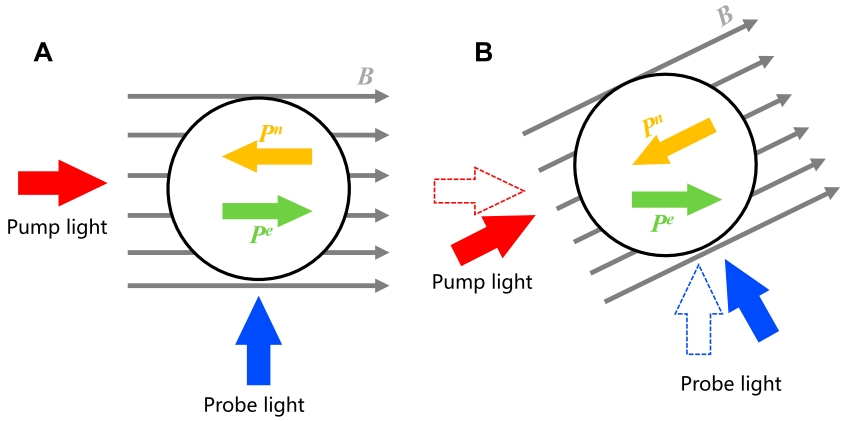

FIGURE 3
Schematic diagram of the operation principle of SERF inertial measurement. **(A)** Initial state of SERF regime; **(B)** Rotation of SERF regime. P^n represents the nuclear spin of the noble and P^e is the electron spin of the alkali metal atom. Due to the strong coupling between the nuclear spin of the noble gas and the electron spin of the alkali metal atom, the nuclear spin of the noble gas can follow and compensate the change of the external magnetic field, so that the static magnetic field felt by the electron spin of the alkali metal atom is close to zero. And the electron spin of the alkali metal atom will only be sensitive to inertial rotation [8].

Major applications and progress of SERF quantum precision measurement

SERF quantum precision measurement has two advantages: ultra-high detection sensitivity and integration of measurement devices. It has broad application prospects in fundamental physics, inertial navigation, biomedicine, geophysics, geomagnetism [28, 29], deep space magnetic detection [30], and extremely weak magnetic detection of matter [31]. At present, SERF quantum precision measurements have the most potential and have made significant research progress in fundamental physics, inertial navigation, and biomedical fields. In the following, we provide a detailed overview of the research in these three application areas.

Fundamental physics

The quantum precision measurement device based on the SERF effect has an important and wide application in measuring basic physical quantities, especially in the new physical research beyond the standard model, because of its ultra-high sensitivity potential. These devices are expected to test the joint symmetry of charge, parity, and time inversion, measure the EDM of particles and detect the spin-spin interaction force. The sensitivity of the SERF measurement device determines the limit of the detection ability of the above physical quantities.

CPT conservation is an important symmetry theory based on the assumption of the standard particle model. The accurate measurement of EDM is conducive to verifying the asymmetry of time inversion. Compared with the method of using a high-energy particle accelerator [32] and large spallation neutron source [33, 34], the SERF measurement device based on atomic spin measures EDM by measuring the precession

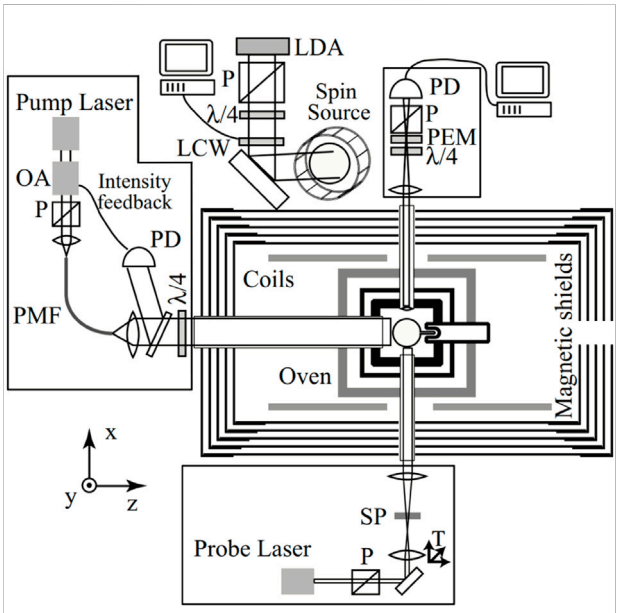

FIGURE 4
Experimental schematic of the first generation horizontal SERF co-magnetometer. Pump light and probe light orthogonally illuminate the cell, which is filled with 12 amagats of ^3He, 46 Torr of N_2 for quenching and a small drop of K [39].

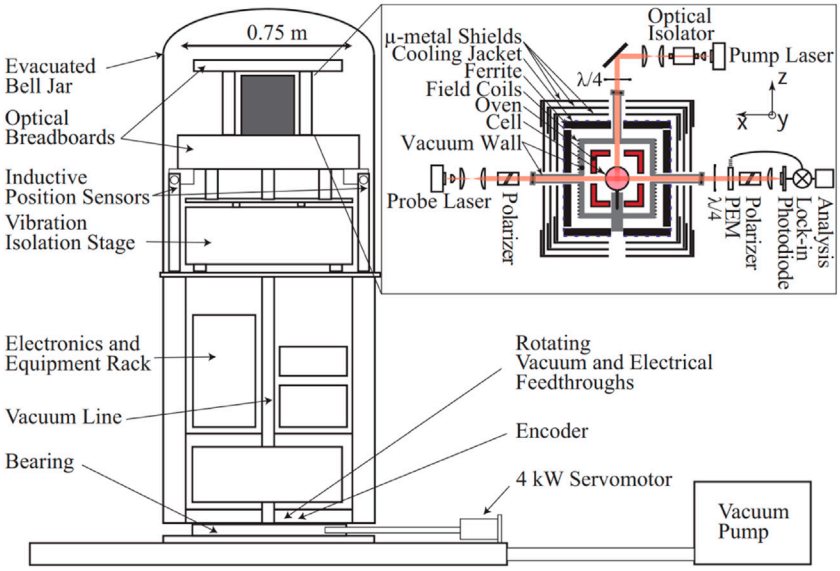

FIGURE 5
Experimental schematic of the second generation vertical SERF co-magnetometer. The cell is filled with 9.4 amagats of ^3He, 29 Torr of N_2 for quenching and a drop of *K*. The optics and associated electronics are mounted on a rotating platform driven by an AC servo motor [42].

signal of particles in the electromagnetic field, which is a more efficient low-energy means [35]. In 2001, Romalis *et al.* measured the EDM of ^{199}Hg using an ultra-high sensitivity experimental device and an ultraviolet laser. The upper limit of the electric dipole moment of 2.1×10^{-28} *e* cm was obtained with a reliability of 95%, which increases the previous EDM limit by 4 times [36]. In 2013, Swallows *et al.* measured the EDM of ^{199}Hg with an improved experimental device including four vapor cells. The upper limit of the EDM of 3.1×10^{-29} *e* cm was obtained with a reliability of 95%, which is an order of magnitude higher than the previous measurement results and 7 times higher than the previous EDM limit [37].

CPT symmetry is broken in the standard model extension theory to some extent [38]. To test CPT symmetry breaking, Allred et al. achieved an atomic spin SERF regime to improve the sensitivity of the device in 2002 [7]. On this basis, the Romalis group demonstrated a new SERF inertial measurement method combined with the high-sensitivity SERF magnetometer in 2005 [13]. Figure 4 shows experimental schematic of the first generation horizontal SERF co-magnetometer, on which Lorentz and CPT tests were carried out. After that, the inertial measurement of the group is divided into engineering applications [39, 40] and Frontier basic physics research [39].

To further test CPT symmetry breaking, the second generation vertical SERF co-magnetometer was designed and built to improve system stability and sensitivity. The experimental device diagram is shown in Figure 5. On the second generation vertical inertial measurement device, Brown et al. studied the neutron spin coupling of Lorentz and CPT destroying under the background field and setting a new limit. The experimental results are 30 times higher than the previous neutron limit and have the highest energy resolution in all spin anisotropy experiments [42, 43].

Because the spin magnetic ratio of the ^{21}Ne atom is one order of magnitude lower than that of the ^{3}He atom, the energy resolution can be improved by one order of magnitude by replacing the ^{3}He atom with the ^{21}Ne atom under the same magnetic field measurement sensitivity. Therefore, the measurement indicators of CPT and Lorenz symmetry breaking and inertial rotation based on ^{21}Ne atom have the potential to increase by an order of magnitude. In addition, the nuclear spin of the ^{21}Ne atom is 3/2, which can be applied to measure the parameters related to tensor interaction in Lorenz symmetry breaking [44]. In 2009, Ghosh *et al.* carried out the preliminary measurement of interaction parameters between ^{21}Ne atom and K atom, and Rb atom, providing support for the application of ^{21}Ne atom in inertial measurement [24, 45]. Based on previous single technology research, Smiciklas *et al.* demonstrated a new K-Rb-^{21}Ne SERF inertial measurement device in 2011, which was used to find tensor interactions that violate local Lorentz invariance. The experimental results showed that the Lorentz failure coefficients in part of the space were limited. These coefficients made the anisotropy uncertainty of particles reach 10^{-29}, and increased the previous limit by 2–4 orders of magnitude [12]. Because the inertial measurement is sensitive to rotation, especially the signal generated by the earth rotation projection will affect the experimental verification of CPT symmetry breaking.

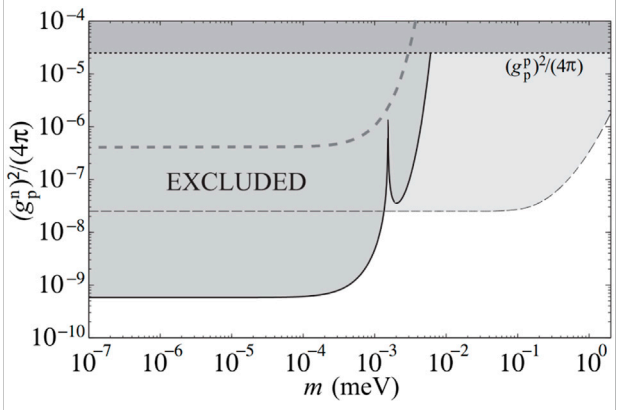

FIGURE 6
Limitations on spin interaction forces in various studies. Constraints on the coupling of pseudoscalar bosons to neutrons as a function of boson mass. Solid lines are from Vasilakis's studies for Yukawa coupling, and other lines are from previous related research [39].

Therefore, Romalis et al. placed the third generation SERF co-magnetometer at the South Pole in 2013, which reduced the previous equivalent ground speed of about 2.6 pT to less than 0.1 fT. To carry out high-precision experimental test of CPT symmetry breaking, they also replaced K atoms with Cs atoms to reduce the optical frequency shift of the system. The inertial measurement sensitivity of this device was 2.8 × $10^{-6°}$/s/$Hz^{1/2}$@ 5Hz, and CPT symmetry-breaking test experiment is currently in progress [46].

In the fifth force detection, the SERF measurement device also plays a great role. In 2009, Vasilakis et al. explored the abnormal nuclear spin-related force generated by a single ^{3}He spin and put forward new restrictions on the abnormal spin force between neutrons. The detection sensitivity for new particles even exceeded the gravity effect, and the inertial angular velocity detection sensitivity of the whole system reached 4.0 × $10^{-6°}$/s/$Hz^{1/2}$@1 Hz. Figure 6 shows the comparison of spin-dependent force limits, and the solid line shows the research results of the team [39]. To find the spin interaction beyond the standard model, Sheng *et al.* described a new ^{3}He-^{129}Xe SERF system detected by Rb atoms and verified a general and practical method through experiments to explore new spin correlation forces in 2014 [47].

In 2018, Lee *et al.* built a K-^{3}He SERF co-magnetometer and applied it to measure the long-range abnormal interaction between fermions. The experimental schematic diagram is shown in Figure 7A. The experimental results increased the limit values of neutrons and electrons by an order of magnitude, as shown in Figures 7B,C [48]. Lee also reported the research progress of SERF atomic spin inertial measurement device of K-Rb-^{21}Ne atomic source used in spin mass interaction limiting experiment [49].

In 2018, Ji et al. reported the search results for long-range spin-spin velocity-dependent forces (SSVDF) based on the $SmCo_5$ spin source and SERF co-magnetometer, and the experimental setup is shown in Figure 8. With the help of a high-sensitivity SERF co-magnetometer, high spin density, and similarity analysis, new constraints on the possible new singular potentials of V_{6+7}, V_8, V_{15}, and V_{16} were derived in the force range of 5 cm − 1 km. In particular, for V_{15}, the experimental results were more than three orders of magnitude better than those of [51] in this force range. For V_8, the experimental results were more than 11 orders of magnitude better than [47] for a force range larger than 1 m. The findings promote the future improvement of SERF sensitivity using similar experimental setups.

In 2020, Almasi et al. built a SERF co-magnetometer based on the Cs-Rb-^{21}Ne ensemble for measuring the anomalous spin-spin interaction between the spin ensemble inside the device and the electron spin source in a $SmCo_5$ magnet, as shown in Figure 9A. The measurements of this device improved the

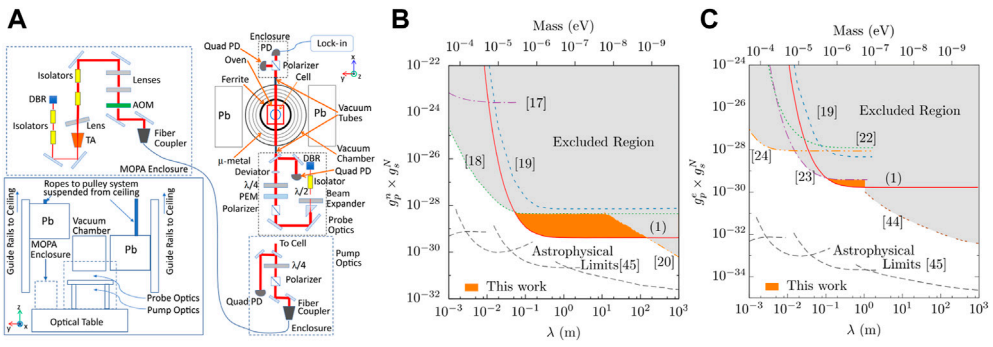

FIGURE 7
(A) Schematic diagram of K-^{3}He co-magnetometer experiment; **(B)** Limit for neutron $g_p^n \times g_s^N$ (95% C.L.); **(C)** Restrictions on electronic $g_p^e \times g_s^N$ (95% C.L.) [48].

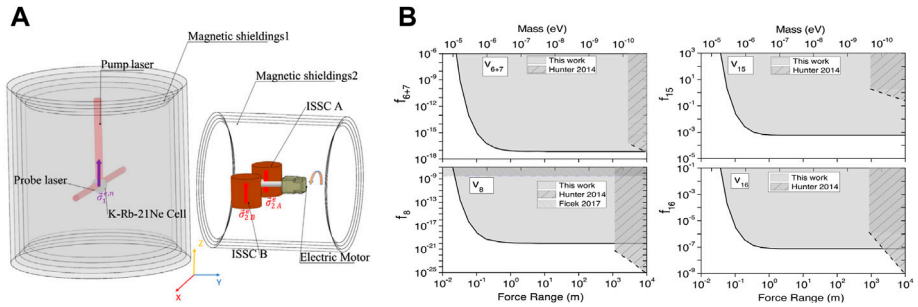

FIGURE 8
(A) Experimental schematic diagram for studying spin-spin velocity-dependent interactions using the SmCo5 spin source; **(B)** Limits on the SSVDFs' coupling constants between two electrons measured (95% C.L.) [50].

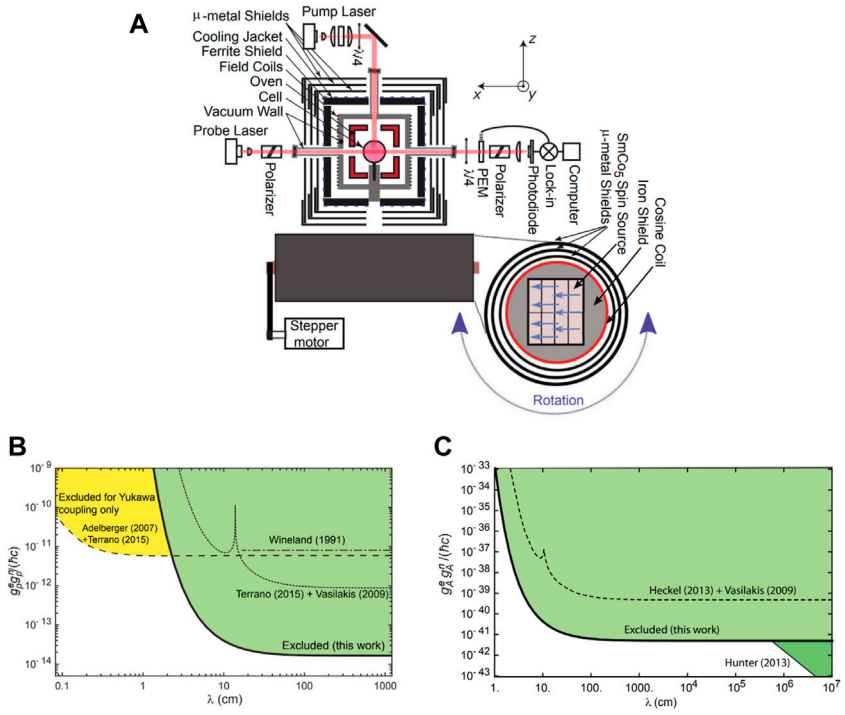

FIGURE 9
(A) Diagram of the experimental setup; **(B)** Constraints on the coupling parameter $g_p^e\ g_p^n$ for the interaction of a pseudoscalar boson with two fermions; **(C)** Constraints on the coupling parameter $g_A^e\ g_A^n$ for the interaction of spin-1 bosons with two fermions [52].

product of the pseudoscalar coupling coefficients of electrons and neutrons by two orders of magnitude, as shown in Figures 9B, C [52].

In 2018, Young et al. investigated the singular spin and velocity-dependent interactions of polarized electrons using a SERF magnetometer. The interaction limit was demonstrated with no periodic signal and an interaction range of 10^{-1} – 10^{-4} m corresponding to 10^{-6} – 10^{-3} eV of the axion mass. This study provided a new direction for axion search [53]. Budker et al. also used SERF magnetometers to study spin interaction and explore new physics such as axions [51, 54]. They led the establishment of a Global Network of Optical Magnetometers (GNOM) project to explore the existence of "anomalous fields" [55]. In 2020 and 2022, Padniuk *et al.* developed the SERF co-magnetometer based on the K-Rb-^{3}He atomic source mainly for the study of GNOME singularity physics [56].

The SERF-based measurement devices dominate fundamental physics research at Princeton University and

push the limits of experimental measurement of physical quantities. Researchers continue improving the sensitivity of the SERF measurement device and exploring fundamental physics research in the direction of dark matter and the fifth force.

Inertial navigation

High-precision inertial measurements have a wide range of applications in navigation [57–59]. Compared with other navigation techniques (e.g. satellite navigation [60], radio navigation [61], geomagnetic navigation [62], and astronomical navigation [63]), inertial navigation has the advantages of high autonomy, real-time continuous navigation information, and high short-time accuracy [64], Currently, the traditional mechanical inertial measurement devices [65–67] and optical inertial measurement devices [68, 69] are the commonly used sensors for inertial navigation. However, due to the limitation of the basic principle, these two types of measurement devices have encountered bottlenecks in further improving performance in applications [27, 70]. With the development of quantum precision measurements, inertial measurements based on atomic spin effects have gradually become a new direction in the field of inertial navigation technology [71, 72]. Quantum precision measurement based on SERF effect can achieve the measurement of carrier angular rate by detecting the Larmor precession angle of atomic spins in a magnetic field [8], and also the measurement device based on this principle can be miniaturized and low-cost by integrating optical and micromachining technologies, so it is considered as an essential development direction for high-precision, small volume and low-cost inertial navigation [73].

The research on SERF quantum precision measurements in the field of inertial navigation started with the development of the SERF atomic spin inertial large-scale measurement device, followed mainly by the exploration of the SERF atomic spin gyroscope. In 2005, based on the research results of the SERF atomic magnetometer, Romalis *et al.* added an inert gas to the alkali metal cell to constitute the K-^{3}He atomic source combined magnetometer [8, 13]. The results show that the device exhibits insensitivity to low-frequency magnetic fields while maintaining ultra-sensitivity to anomalous fields and rotational angular rates, thus achieving the world's first proof-of-principle for atomic spin inertia measurements based on the SERF effect. Using this research device, they achieved an inertial measurement sensitivity of 2.9×10^{-5}°/s/Hz$^{1/2}$ and a zero bias stability index of 0.04°/h. Subsequently, based on the first-generation device, the group developed a second-generation SERF atomic co-magnetometer [12]. And they measured the angular rate of the Earth's rotation and finally achieved an inertial measurement sensitivity of 8.6×10^{-6} rad/s/Hz$^{1/2}$@0.2 Hz [42, 43].

Later, Romalis et al. explored the ^{21}Ne atomic source scheme and measured the relevant system parameters. They proposed a hybrid pumping-based K-Rb-^{21}Ne source scheme to suppress the polarization gradient and improve the polarization efficiency of the atomic spins, which again improved the inertial measurement sensitivity, eventually achieving an inertial measurement sensitivity of 1.2×10^{-5} rad/s/Hz$^{1/2}$@0.2 Hz [74]. In 2013, Romalis et al. set up a corresponding measurement device at the South Pole for testing. The device used a Cs-Rb-^{21}Ne atomic source scheme with a Cs-Rb hybrid optical pumping technique to reduce the polarization gradient of alkali metal atoms and enhance the polarization efficiency of noble gases [46] to finally achieve an inertial measurement sensitivity of 3.6×10^{-6} rad/s/Hz$^{1/2}$@0.2 Hz [46]. The group in French Aerospace Laboratory carried out the Studies on SERF atomic co-magnetometer based on the Rb-^{129}Xe atomic source [75]. However, related performance metrics and subsequent progress were not reported.

In addition to the atomic source, subsequent studies have targeted other parts of the inertial measurement system for optimization to enhance the inertial measurement performance further. In 2019, Jiang *et al.* investigated the effect of pump laser power density on SERF inertial measurements [76]. The experimental setup and analysis are shown in Figure 10. The results show that the suppression and long-term stability of low-frequency magnetic noise improve with increasing pump laser power density due to the increased nuclear spin polarization. Jiang *et al.* also proposed the first real-time closed-loop control of the nuclear spin self-compensation point in SERF inertial measurements, which improves the system stability and extends the linear measurement range by locking the electron resonance. Alkali metal electrons are not affected by the longitudinal ambient magnetic field fluctuations and nuclear magnetization [77]. In 2020, Huang et al. studied the laser polarization error of the detection system in the SERF inertial measurement device [78]. They established the optical transmission model of the detection system by using the Jones matrix about the optical defects of the polarizer. Then the polarization error was analyzed based on the model, and a new error suppression method was proposed, which can finally improve the long-term performance of SERF inertial measurements by about 3.4 times.

Based on the proof-of-principle using large measurement devices, SERF quantum precision inertial measurements have been developed toward small-scale integration, and SERF atomic spin gyroscopes suitable for practical use in inertial navigation have been widely studied. In 2017, the Romalis group participated in a chip-scale combined atomic navigator program with Twinleaf to develop a low-drift nuclear spin gyro. They developed an atomic spin gyroscope on the ^{87}Rb-^{3}He-^{129}Xe atomic source. A bias instability of less than

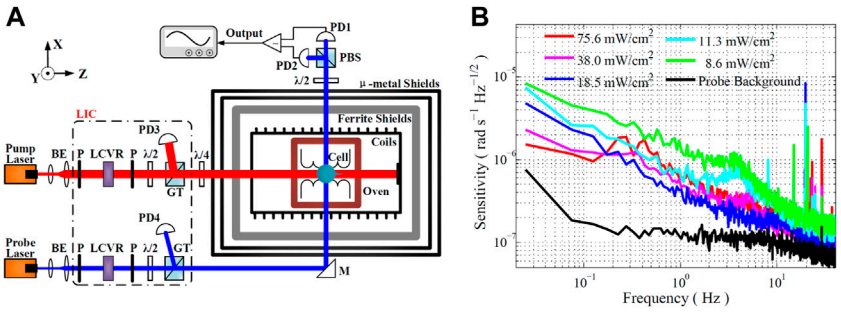

FIGURE 10
(A) Schematic of compact SERF comagnetometer using K-Rb hybrid optical pumping; **(B)** Rotation sensitivity of the comagnetometer operated at different pump laser power density [76].

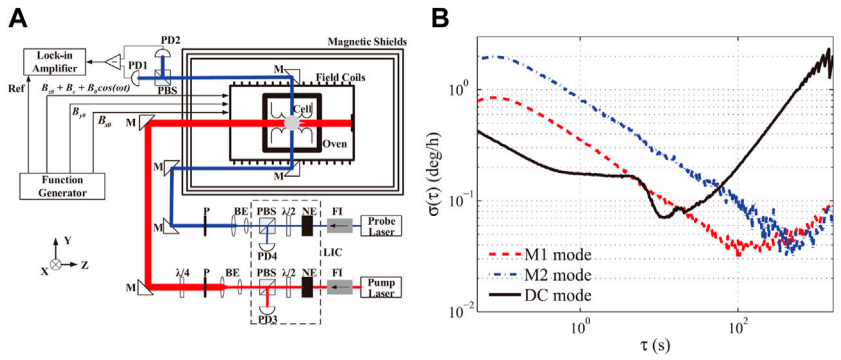

FIGURE 11
(A) Experimental setup of the dual-axis atomic spin gyroscope; **(B)** Allan deviation plots of the modulated dual-axis gyroscope (M1 mode:Using the lock-in amplifier to demodulate and detect the double frequency signal output by the laser; M2 mode: Using the lock-in amplifier to demodulate and detect the double frequency signal output by the laser.) and the unmodulated mode gyroscope [79].

0.01°/h was achieved using a 10 mm diameter spherical cell. And a bias instability of better than 0.2°/h was demonstrated by a 2 mm diameter cell made by anodic bonding. Twinleaf also developed an extensive miniaturization and integration technology for the prototype and developed a prototype with a volume of only 1.6 cm^3, including the cell, heater, and VCSEL. And the bias instability of 3°/h was achieved [41].

In 2018, Jiang et al. described a dual-axis SERF atomic spin gyroscope based on an alkali metal-noble gas co-magnetometer [79]. They utilized longitudinal high-frequency magnetic field modulation instead of polarization modulators in operation. By using a parametric modulation technique, the low-frequency drift is effectively suppressed, resulting in a bias instability of less than 0.05°/h. The constructed experimental setup and experimental results are shown in Figure 11.

In 2019, Fan et al. investigated the bias error caused by magnetic noise in SERF atomic spin gyroscopes [80]. They demonstrated that the thermal magnetization noise in the ferrite shield limits the performance of inertial measurements. The root cause of this error is the low-frequency magnetic field sensitivity dominated by the nuclear spin relaxation rate, which can be reduced to achieve the ultimate noise suppression. The experimental setup and noise analysis are shown in Figure 12. Fan et al. also proposed a new method to suppress the bias error caused by the fluctuation of the probe light intensity in the SERF atomic spin gyroscope, and the superiority of this method was demonstrated on the joint K-Rb-^{21}Ne magnetometer. A bias stability of about 0.01°/h was obtained. This method can eliminate the requirement for closed-loop control of the probe light intensity, thus facilitating the miniaturization of the gyroscope size and reliability [81].

In addition, Twinleaf has applied for two patents which are circuit board integrated atomic gyroscopes and atomic modulated low drift sensors [39, 41]. The first patent proposes a new integration scheme for miniaturized atomic magnetometers and gyroscopes, and the second patent demonstrates a miniaturized atomic magnetometer and gyroscope magnetic field modulation detection scheme.

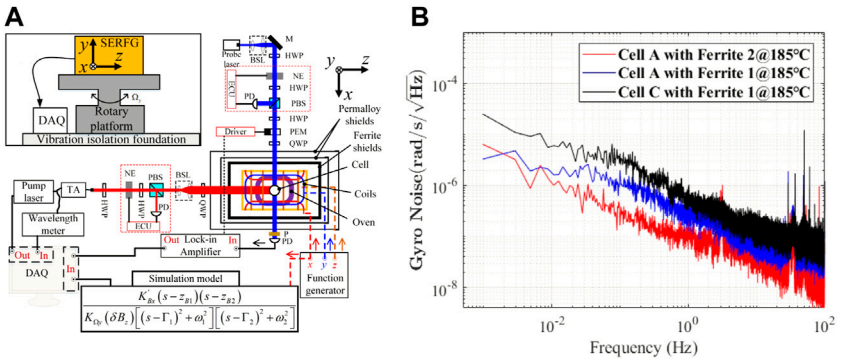

FIGURE 12
(A) Schematic diagram of the prototype of Fan's research. The experimental device consists of sensitivity source, magnetic field control system, optical pumping and detection system, electronic control and signal acquisition system; **(B)** Noises of the cells at dierent neon pressures at 185°C [80].

Honeywell also has conducted research related to chip-scale SERF atomic spin gyroscopes and designed the corresponding structures and process implementation methods. SERF quantum precision measurement in the field of inertial navigation has progressed towards high accuracy, downsizing, and cheap cost to satisfy the needs of long-term autonomous navigation, and is expected to be widely used in the military and aerospace fields in the future.

Biomedicine

During the development of magnetic field detection, the quantum precision measurement device based on the SERF effect is a research hotspot. While the magnetic field measurement sensitivity is improved, the volume of the measurement device is also shrinking. This development trend has laid a foundation for its application in the biomedical field. Biological extremely weak magnetic measurement based on SERF precision measurement has developed rapidly, especially the measurement of human cardiac magnetic field and brain magnetic field has become a research hotspot in recent years. Superconducting quantum interferometer device (SQUID) is usually used for direct measurement of cardiac magnetic field and brain magnetic field signals [82], but its application is greatly limited by the high maintenance cost and liquid helium Dewar bottle of superconducting refrigeration [83, 84]. Fortunately, the SERF atomic magnetometer can realize ultra-high precision magnetic field measurement, and has the advantages of no need for low-temperature cooling, wearable human body and mobile measurement, which makes it greatly developed in the field of biological magnetic field detection such as human cardiac magnetism and brain magnetism [9, 10].

In 2012, Kamada et al. used the high-sensitive SERF potassium atomic magnetometer to collect human cardiac magnetic field signals, which was consistent with the results measured by SQUID, which proved the potential of the magnetometer in biomagnetic measurement [85]. Wyllie et al. proposed a portable and modular four-channel SERF magnetometer array device to improve the adaptability of magnetometer configuration to biological magnetic field signals and used the device to measure adult magnetocardiography (MCG), as shown in Figure 13 [86].

In 2019, Sulai et al. used two SERF optically pumped magnetometers (OPMs) to form a gradiometer to optimize the background noise and carried out research on possible detection problems of fetal magnetocardiography measurement [87]. In 2020, Zhang et al. also used the gradiometer composed of two SERF magnetometers to suppress common-mode noise, and successfully measured cardiac magnetic field signals, which proved that the OPM gradiometer can be used for the measurement of biomagnetic signals [88]. In 2021, Yang et al. developed a wearable multi-channel magnetocardiography system based on the SERF magnetometer array and measured the magneto cardiograms signal, which provided a realizable device for cardiac electromagnetic activity imaging, as shown in Figure 14 [89]. In 2022, Zhang et al. proposed a simple optical method to solve complex electronic control problems, which realized a VCSEL integrated SERF magnetometer and measured the cardiac magnetic field signal. This work provides a new way to develop the VCSEL integrated SERF magnetometer and apply it to magnetoencephalography (MEG) [90].

Although the brain magnetic field signal is about 100 times weaker than the cardiac magnetic field signal, it contains more medical information, so the measurement and application of

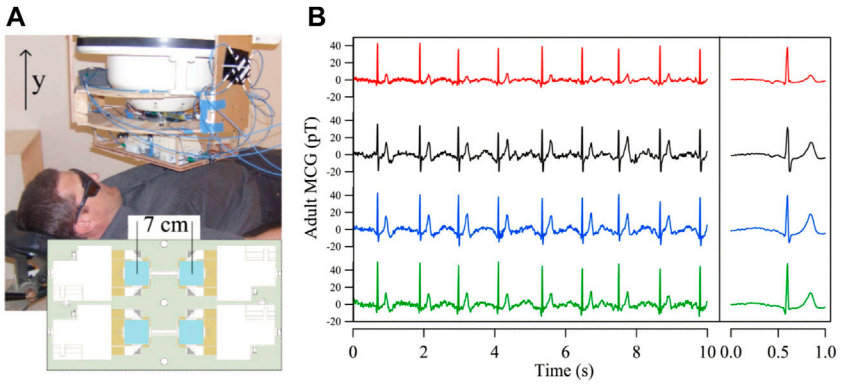

FIGURE 13
(A) Four-channel SERF magnetometer array with 7 cm channel spacing; **(B)** Four-channel adult MCG with large signal interferences subtracted and the same set of MCG after averaging each channel [86].

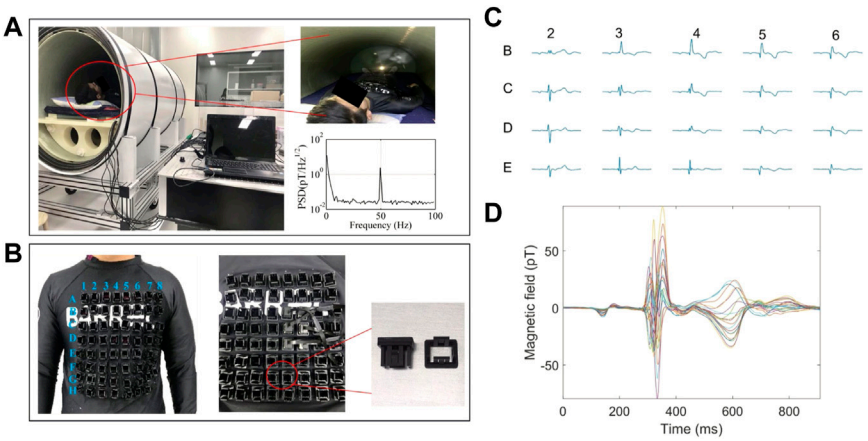

FIGURE 14
(A) Magnetically shielded cylinder and magnetic noise spectrum; **(B)** Position labels of the 8 × 8 array with 30 mm intervals, QZFM magnetometer and customized receptacles; **(C)** The MCG preprocessed at the 20 spatial locations for a single epoch (unaveraged); **(D)** Butterfy of MCG [89].

the brain magnetic field signal are more extensive. In 2003, Kominis et al. successfully obtained the brain magnetic field signal through the gradiometer composed of a multi-channel SERF magnetometer, which made it possible to study the cerebral cortex module non-invasively [22]. In 2006, Xia et al. developed the principle prototype of SERF magnetometer applied to improve the spatial resolution of magnetic field measurement using magnetoencephalography. The magnetometer adopted a ×16 16 pixel array photodetectors which increased the number of measurement channels to 256 and realized the two-dimensional magnetoencephalogram drawing of the human auditory evoked test, as shown in Figure 15 [91].

In 2010, Johnson et al. proposed a SERF magnetometer for pumping light and detecting photosynthetic beams, and successfully detected the brain magnetic field response signals of the median nerve and auditory stimulation [92]. In 2013, the group measured the auditory stimulus-evoked signals of subjects with a multi-channel SERF magnetometer and used multi-channel signal processing technology to improve the signal quality. This work was the first demonstration of using a multi-channel SERF magnetometer to realize brain magnetic imaging, providing a framework for an array magnetometer to be used for brain magnetic imaging positioning [93]. Shah et al. proposed a high-sensitivity SERF magnetometer applied to biomedicine to measure the brain magnetic field signal, and

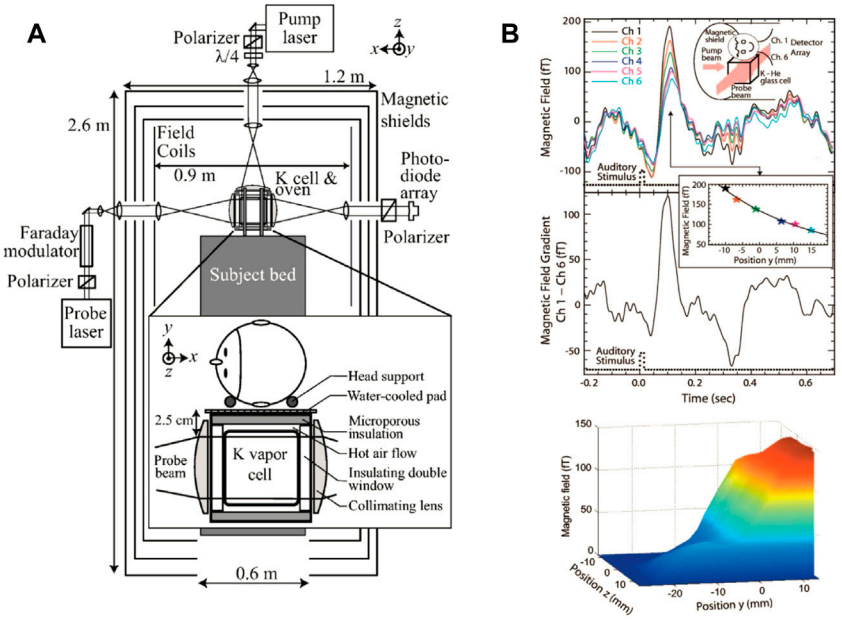

FIGURE 15
(A) Experimental schematic diagram of MEG system; **(B)** Auditory evoked magnetic fields obtained with atomic magnetometer after averaging 600 stimuli presentations [91].

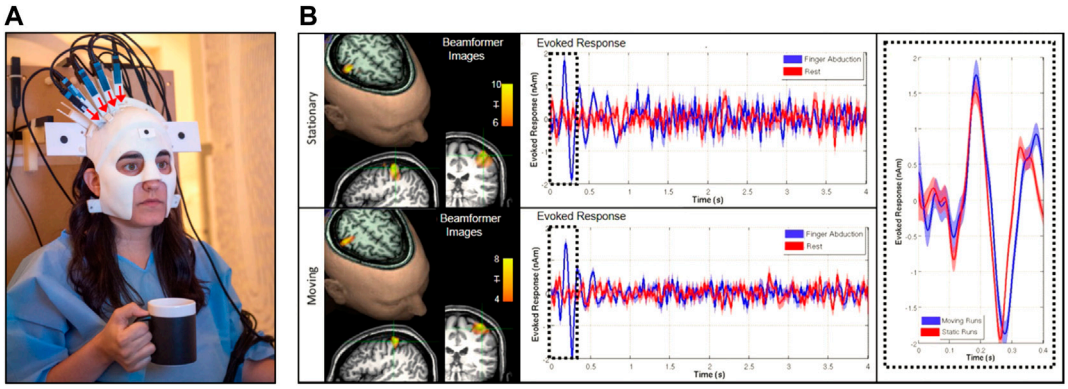

FIGURE 16
(A) The prototype OPM-MEG system helmet, which is customized with sensors directly close to the surface of the scalp; **(B)** Evoked response analysis in MEG [84].

the measured signals using SERF magnetometer and SQUID were compared to cross verify the feasibility of the device based on the SERF atomic magnetometer to measure the brain magnetic field [94]. In 2014, Kim et al. measured the auditory evoked field in the human brain with a multi-channel atomic magnetometer system and realized the positioning of dipole phantom and auditory evoked field [95]. In 2017, Sheng et al. demonstrated a SERF magnetometer based on alkali Cs and verified the performance of the magnetometer by referring to the auditory evoked the brain magnetic field signals of the SQUID channel. This magnetometer required a lower heating temperature and may be used to build a multi-channel array magnetometer for neuroscience research [96]. In 2018, the University of Nottingham developed a new wearable MEG

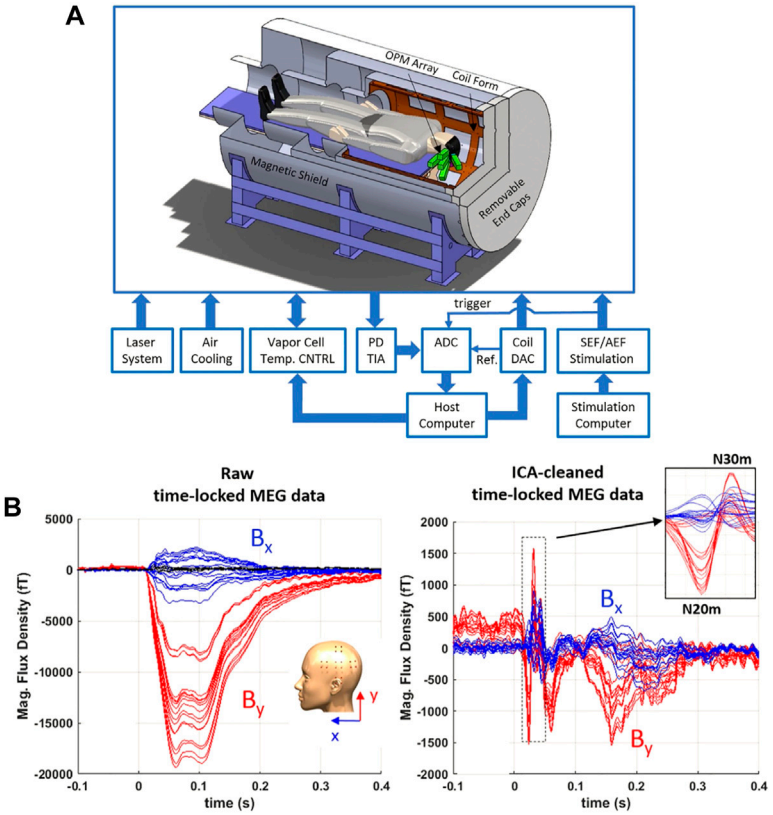

FIGURE 17
(A) Block diagram of MEG system including a drawing of the magnetic shield containing the subject and OPM array; **(B)** Evoked responses elicited by median nerve stimulation showing horizontal and vertical field components from 20 channels [100].

system by using the first generation SERF magnetometer of Quspin company, which was used to measure the electrophysiological signals of subjects with millisecond resolution under natural motion, as shown in Figure 16. This work opens up new possibilities for MEG to be applied to any subject and patient group [84].

In 2019, Du et al. measured the steady-state visual evoked potential of a healthy subject with a gradiometer composed of a compact four-channel SERF magnetometer, proving the application potential of the MEG system constructed by the gradiometer in biological magnetic field measurement and brain-computer interface [97]. To meet the requirement that the SERF magnetometer can simultaneously measure the signals of multiple locations in the human brain, Zhang et al. developed a SERF magnetometer for multi-channel biaxial vector magnetic field measurement in a single cell, and used a ×22 photodiode matrix to measure the two-dimensional spatial magnetic field distribution. And the auditory evoked magnetic fields were detected simultaneously at four adjacent locations perpendicular to the scalp [98]. In 2020, Borna et al. built a 20-channel array-type brain magnetic functional imaging measurement device by using five 4-channel second-generation principle prototypes. They studied the auditory evoked magnetic field and somatosensory evoked magnetic field and cross-verified with the SQUID-based brain magnetic mapping system to achieve sub-centimeter precision magnetic source positioning, which provided the possibility for the MEG system with full head coverage of a compatible and flexible OPM sensor array [99, 100], as shown in Figure 17. The group also discussed the influence of horizontal axis projection error on the positioning and calibration accuracy of MEG system [10].

In 2020, Zhang et al. introduced an unshielded MEG system based on SERF magnetometers. The magnetometer worked in gradient and closed-loop feedback mode to reduce the environmental magnetic field noise. The system successfully measured the auditory evoked field signal and alpha rhythm signal related to eye closure under the unshielded earth's magnetic field, which was expected to achieve a movable and wearable unshielded MEG system [101]. Quspin cooperating with the University of Nottingham developed a 49-channel whole-brain wearable magnetoencephalogram system [102] by using the second

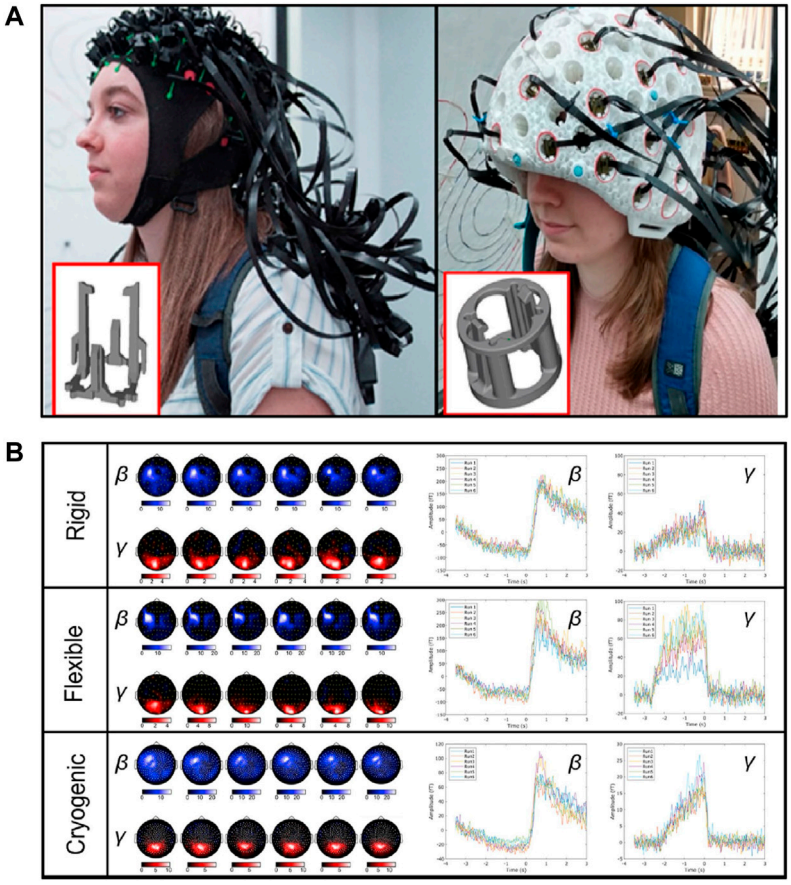

FIGURE 18
(A) A multi-channel whole brain wearable MEG system (flexible helmet and rigid helmet); **(B)** Sensor-space beta- and gamma-band signals [102].

generation of SERF magnetometer, as shown in Figure 18. The system was placed in a custom-made magnetic shielding room. The sensors were fixed by using a rigid helmet and a flexible head cover. Combined with the large biplane coil dynamic magnetic field compensation technology [103], the β and γ waves of brain were measured. This work further proves that MEG may be used in functional neuroimaging. In addition, focal epilepsy, auditory evoked field under sitting and standing conditions and electrically induced muscle response were also performed based on the SERF magnetometer [104–107].

In 2021, Cao et al. compared the co-registration accuracy of the three devices used for the co-registration of on-scalp MEG and magnetic resonance imaging (MRI) in detail and proposed a reference model to quantify the co-registration performance of each device, which provided some suggestions and considerations for researchers to select and use appropriate devices for the co-registration of on-scalp MEG and MRI [108]. In 2022, An et al. proposed a new parameterized method to estimate the number of magnetic sources and locate multiple magnetic sources, which was used in the 31-channel MEG system. The feasibility of this method was verified by measuring the brain magnetic field signals through multi-mode sensory stimulation experiments [109]. Then, a spatial smoothing estimation method based on variational free energy was also proposed to improve the accuracy of somatosensory cortical response, and a 32-channel OPM-MEG system was constructed to measure the response of the cerebral cortex to the median and ulnar nerve stimulation [110]. Theoretical and experimental studies showed that the SERF magnetometer which can provide complete three-axis vector magnetic field information will help to improve the performance of the OPM-MEG system [111, 112]. Tang et al. put forward a variety of schemes to realize the three-axis magnetic field vector measurement of the SERF magnetometer, which will promote a large number of applications of the three-axis SERF magnetometer in the OPM-MEG system [113, 114].

Throughout the development of SERF quantum precision measurement in biomedicine, from the initial laboratory principle prototype to the multi-channel miniaturized probe, and then to the integrated medical device, it is developing vigorously toward high-resolution biological magnetic field imaging [115]. It is believed that the OPM-MEG can fully replace the SQUID-MEG system in the future [116], and it will become a powerful tool for medical diagnosis and neurofunctional cognition.

Conclusion

In summary, quantum precision measurement based on the SERF effect has ultra-high detection sensitivity, which makes it have broad application prospects in many fields such as fundamental physics, inertial navigation, and biomedicine. We have reviewed its research progress and applications and find that there are two trends in its development: one is to continuously improve the detection sensitivity by developing large-scale SERF measurement devices for Frontier physical sciences; the other is to develop integrated SERF measurement devices, focusing on improving detection stability or detection resolution, which can be widely used in inertial navigation, biomedicine, geomagnetic measurements, *etc.*

At present, quantum precision measurement based on the SERF effect has not yet reached the theoretical limit of measurement, and continuous improvement of detection sensitivity is still one of the critical research content in the future. In addition, compared with large SERF measurement devices, integrated SERF measurement devices have more significant application potential. The following research directions are for integrated SERF measurement devices, new detection techniques in unshielded geomagnetic environments and microfabrication techniques.

Author contributions

YZ conceived the idea. YL organized the article. All authors contributed to the writing of the manuscript. All authors reviewed the manuscript.

References

1. Li R, Baynes FN, Luiten AN, Perrella C. Continuous high-sensitivity and high-bandwidth atomic magnetometer. *Phys Rev Appl* (2020) 14:064067. doi:10.1103/physrevapplied.14.064067

2. Hou Z, Zhang Z, Xiang GY, Li CF, Guo GC, Chen H, et al. Minimal tradeoff and ultimate precision limit of multiparameter quantum magnetometry under the parallel scheme. *Phys Rev Lett* (2020) 125:020501. doi:10.1103/PhysRevLett.125.020501

3. Hu D, Niu L, Jin S, Chen X, Dong G, Schmiedmayer J, et al. Ramsey interferometry with trapped motional quantum states. *Commun Phys* (2018) 1:1–9. doi:10.1038/s42005-018-0030-7

4. Shao H, Huang Y, Guan H, Li C, Shi T, Gao K. Precise determination of the quadrupole transition matrix element of ca+ 40 via branching-fraction and lifetime measurements. *Phys Rev A* (2017) 95:053415. doi:10.1103/physreva.95.053415

5. Chupp T, Fierlinger P, Ramsey-Musolf M, Singh J. Electric dipole moments of atoms, molecules, nuclei, and particles. *Rev Mod Phys* (2019) 91:015001. doi:10.1103/revmodphys.91.015001

6. Bohnet JG, Cox KC, Norcia MA, Weiner JM, Chen Z, Thompson JK. Reduced spin measurement back-action for a phase sensitivity ten times beyond the standard quantum limit. *Nat Photon* (2014) 8:731–6. doi:10.1038/nphoton.2014.151

Funding

This work was supported by the National Natural Science Foundation of China (Grant No. 62003020) and the Key Research and Development Program of Zhejiang, China (Grant No. 2020C01037).

Acknowledgments

We would like to give this paper to Professor Wang Yiqiu, and thank him for his guidance in scientific research and help in life for the authors over the years. Professor Wang Yiqiu is a pioneer in the field of time and frequency measurement in China, especially in frequency standards. At the same time, Professor Wang has actively cultivated a large number of leading talents in the field of quantum precision measurement and quantum simulation, including Professor Chen Xuzong and Professor Zhou Xiaoji. During his doctoral studies at Peking University, the author asked Professor Wang for advice many times. Professor Wang's profound understanding of physics has greatly benefited the author. It is hoped that under the leadership of Professor Wang and other outstanding scholars, the study field of light-atomic interaction in China will make rapid progress.

Conflict of interest

The authors declare that the research was conducted in the absence of any commercial or financial relationships that could be construed as a potential conflict of interest.

Publisher's note

7. Allred J, Lyman R, Kornack T, Romalis MV. High-sensitivity atomic magnetometer unaffected by spin-exchange relaxation. *Phys Rev Lett* (2002) 89: 130801. doi:10.1103/physrevlett.89.130801

8. Kornack T, Ghosh R, Romalis MV. Nuclear spin gyroscope based on an atomic comagnetometer. *Phys Rev Lett* (2005) 95:230801. doi:10.1103/physrevlett.95.230801

9. Hill RM, Devasagayam J, Holmes N, Boto E, Shah V, Osborne J, et al. Using opm-meg in contrasting magnetic environments. *NeuroImage* (2022) 253:119084. doi:10.1016/j.neuroimage.2022.119084

10. Borna A, Iivanainen J, Carter TR, McKay J, Taulu S, Stephen J, et al. Cross-axis projection error in optically pumped magnetometers and its implication for magnetoencephalography systems. *NeuroImage* (2022) 247:118818. doi:10.1016/j.neuroimage.2021.118818

11. Zhang X, Qin J, Wang Y, Chen C. A fast identification on the spin-exchange relaxation-free regime of atomic magnetometer exploiting measurement on gyromagnetic ratio. *IEEE Trans Instrumentation Meas* (2018) 68:1157–64.

12. Smiciklas M, Brown J, Cheuk L, Smullin S, Romalis MV. New test of local lorentz invariance using aNe21–Rb–KComagnetometer. *Phys Rev Lett* (2011) 107: 171604. doi:10.1103/physrevlett.107.171604

13. Kornack TW. *A test of CPT and Lorentz symmetry using a potassium-helium-3 co-magnetometer*. Princeton, NJ, USA: Princeton University (2005).

14. Romalis M, Kornack T. Chip-scale combinatorial atomic navigator (c-scan) low drift nuclear spin gyroscope. In: *Tech. rep*. Princeton, NJ, USA: Princeton University Princeton United States (2018).

15. Dehmelt H. Modulation of a light beam by precessing absorbing atoms. *Phys Rev* (1957) 105:1924–5. doi:10.1103/physrev.105.1924

16. Bell WE, Bloom AL. Optical detection of magnetic resonance in alkali metal vapor. *Phys Rev* (1957) 107:1559–65. doi:10.1103/physrev.107.1559

17. Haji-Sheikh MJ, Allen K. Anisotropic magnetoresistance (amr) magnetometers. In: *High sensitivity magnetometers*. Berlin, Germany: Springer (2017). p. 167–99. doi:10.1007/978-3-319-34070-8_6

18. Happer W, Tang H. Spin-exchange shift and narrowing of magnetic resonance lines in optically pumped alkali vapors. *Phys Rev Lett* (1973) 31: 273–6. doi:10.1103/physrevlett.31.273

19. Happer W, Tam A. Effect of rapid spin exchange on the magnetic-resonance spectrum of alkali vapors. *Phys Rev A* (1977) 16:1877–91. doi:10.1103/physreva.16.1877

20. Seltzer SJ. *Developments in alkali-metal atomic magnetometry*. Princeton, NJ, USA: Princeton University (2008).

21. Anderson LW, Pipkin FM, Baird JC, Jr. Hyperfine structure of hydrogen, deuterium, and tritium. *Phys Rev* (1960) 120:1279–89. doi:10.1103/physrev.120.1279

22. Kominis I, Kornack T, Allred J, Romalis MV. A subfemtotesla multichannel atomic magnetometer. *Nature* (2003) 422:596–9. doi:10.1038/nature01484

23. Fan W, Liu G, Li R, Quan W, Jiang L, Duan L. A three-axis atomic magnetometer for temperature-dependence measurements of fields in a magnetically shielded environment. *Meas Sci Technol* (2017) 28:095007. doi:10.1088/1361-6501/aa7888

24. Ghosh RK. *Spin exchange optical pumping of neon and its applications*. Princeton, NJ, USA: Princeton University (2009).

25. Li Z, Wakai RT, Walker TG. Parametric modulation of an atomic magnetometer. *Appl Phys Lett* (2006) 89:134105. doi:10.1063/1.2357553

26. Budker D, Gawlik W, Kimball D, Rochester S, Yashchuk V, Weis A. Resonant nonlinear magneto-optical effects in atoms. *Rev Mod Phys* (2002) 74:1153–201. doi:10.1103/revmodphys.74.1153

27. Stoner R, Walsworth R. Collisions give sense of direction. *Nat Phys* (2006) 2: 17–8. doi:10.1038/nphys204

28. Tartaglia A, Di Virgilio A, Belfi J, Beverini N, Ruggiero ML. Testing general relativity by means of ring lasers. *The Eur Phys J Plus* (2017) 132:1–10. doi:10.1140/epjp/i2017-11372-5

29. Schreiber KU, Klügel T, Wells JP, Hurst R, Gebauer A. How to detect the chandler and the annual wobble of the Earth with a large ring laser gyroscope. *Phys Rev Lett* (2011) 107:173904. doi:10.1103/physrevlett.107.173904

30. Díaz-Michelena M. Small magnetic sensors for space applications. *Sensors* (2009) 9:2271–88. doi:10.3390/s90402271

31. Romalis MV, Dang HB. Atomic magnetometers for materials characterization. *Mater Today* (2011) 14:258–62. doi:10.1016/s1369-7021(11)70140-7

32. Flambaum V, Pospelov M, Ritz A, Stadnik Y. Sensitivity of edm experiments in paramagnetic atoms and molecules to hadronic c p violation. *Phys Rev D* (2020) 102:035001. doi:10.1103/physrevd.102.035001

33. McClintock DA, Riemer BW, Ferguson PD, Carroll AJ, Dayton MJ. Initial observations of cavitation-induced erosion of liquid metal spallation target vessels at the spallation neutron source. *J Nucl Mater* (2012) 431:147–59. doi:10.1016/j.jnucmat.2011.11.021

34. Wakui T, Wakai E, Naoe T, Shintaku Y, Li T, Murakami K, et al. Recent studies for structural integrity evaluation and defect inspection of j-parc spallation neutron source target vessel. *J Nucl Mater* (2018) 506:3–11. doi:10.1016/j.jnucmat.2018.02.030

35. Griffith W, Swallows M, Loftus T, Romalis M, Heckel B, Fortson E. Improved limit on the permanent electric dipole moment ofHg199. *Phys Rev Lett* (2009) 102: 101601. doi:10.1103/physrevlett.102.101601

36. Romalis M, Griffith W, Jacobs J, Fortson E. New limit on the permanent electric dipole moment of199Hg. *Phys Rev Lett* (2001) 86:2505–8. doi:10.1103/physrevlett.86.2505

37. Swallows M, Loftus T, Griffith W, Heckel B, Fortson E, Romalis MV. Techniques used to search for a permanent electric dipole moment of the 199 hg atom and the implications for cp violation. *Phys Rev A* (2013) 87: 012102. doi:10.1103/physreva.87.012102

38. Colladay D, Kostelecký VA. CPTviolation and the standard model. *Phys Rev D* (1997) 55:6760–74. doi:10.1103/physrevd.55.6760

39. Vasilakis G, Brown J, Kornack T, Romalis M. Limits on new long range nuclear spin-dependent forces set with aK–He3Comagnetometer. *Phys Rev Lett* (2009) 103:261801. doi:10.1103/physrevlett.103.261801

40. [Dataset] Kornack TW, Foley EL. *System and method for atom-modulated, low-drift sensor*. US Patent 9,575,144 (2017).

41. [Dataset] Foley EL, Kornack TW. *Circuit board integrated atomic magnetometer and gyroscope*. US Patent 9,638,768 (2017).

42. Brown J, Smullin S, Kornack T, Romalis M. New limit on lorentz- andCPT-violating neutron spin interactions. *Phys Rev Lett* (2010) 105:151604. doi:10.1103/physrevlett.105.151604

43. Brown JM. *A new limit on Lorentz-and CPT-violating neutron spin interactions using a potassium-Helium comagnetometer*. Princeton, NJ, USA: Princeton University (2011).

44. Chupp T, Hoare R, Loveman R, Oteiza E, Richardson J, Wagshul ME, et al. Results of a new test of local lorentz invariance: A search for mass anisotropy inNe21. *Phys Rev Lett* (1989) 63:1541–5. doi:10.1103/physrevlett.63.1541

45. Ghosh RK, Romalis MV. Measurement of spin-exchange and relaxation parameters for polarizing ne 21 with k and rb. *Phys Rev A* (2010) 81:043415. doi:10.1103/physreva.81.043415

46. Smiciklas M, Vernaza A, Romalis M. Test of lorentz invariance at the amundsen-scott south pole station. *Bull Am Phys Soc* (2013) 58.

47. Sheng D, Kabcenell A, Romalis MV. New classes of systematic effects in gas spin comagnetometers. *Phys Rev Lett* (2014) 113:163002. doi:10.1103/physrevlett.113.163002

48. Lee J, Almasi A, Romalis M. Improved limits on spin-mass interactions. *Phys Rev Lett* (2018) 120:161801. doi:10.1103/physrevlett.120.161801

49. Lee J. *New constraints on the axion's coupling to nucleons from a spin mass interaction limiting experiment (SMILE)*. Ph.D. thesis. Princeton, NJ, USA: Princeton University (2019).

50. Ji W, Chen Y, Fu C, Ding M, Fang J, Xiao Z, et al. New experimental limits on exotic spin-spin-velocity-dependent interactions by using SmCo5 spin sources. *Phys Rev Lett* (2018) 121:261803. doi:10.1103/physrevlett.121.261803

51. Wang T, Kimball DFJ, Sushkov AO, Aybas D, Blanchard JW, Centers G, et al. Application of spin-exchange relaxation-free magnetometry to the cosmic axion spin precession experiment. *Phys dark universe* (2018) 19:27–35. doi:10.1016/j.dark.2017.11.003

52. Almasi A, Lee J, Winarto H, Smiciklas M, Romalis MV. New limits on anomalous spin-spin interactions. *Phys Rev Lett* (2020) 125:201802. doi:10.1103/physrevlett.125.201802

53. Kim YJ, Chu PH, Savukov I. Experimental constraint on an exotic spin- and velocity-dependent interaction in the sub-meV range of axion mass with a spin-exchange relaxation-free magnetometer. *Phys Rev Lett* (2018) 121:091802. doi:10.1103/PhysRevLett.121.091802

54. Safronova M, Budker D, DeMille D, Kimball DFJ, Derevianko A, Clark CW. Search for new physics with atoms and molecules. *Rev Mod Phys* (2018) 90:025008. doi:10.1103/revmodphys.90.025008

55. Afach S, Budker D, DeCamp G, Dumont V, Grujić ZD, Guo H, et al. Characterization of the global network of optical magnetometers to search for exotic physics (gnome). *Phys Dark Universe* (2018) 22:162–80. doi:10.1016/j.dark.2018.10.002

56. Padniuk M, Kopciuch M, Cipolletti R, Wickenbrock A, Budker D, Pustelny S. *Self-compensating co-magnetometer vs. spin-exchange relaxation-free*

magnetometer: Sensitivity to nonmagnetic spin couplings (2021). *arXiv preprint arXiv:2107.05501*.

57. Morton YJ, van Diggelen F, Spilker JJ, Jr, Parkinson BW, Lo S, Gao G. *Position, navigation, and timing technologies in the 21st century: Integrated satellite navigation, sensor systems, and civil applications*. Hoboken, NJ, USA: John Wiley & Sons (2021).

58. Barbour NM. Inertial navigation sensors. In: *Tech. rep*. Cambridge, MA, USA: Charles Stark Draper Lab Inc Cambridge Ma (2010).

59. King A. Inertial navigation-forty years of evolution. *GEC Rev* (1998) 13:140–9.

60. Li R, Zheng S, Wang E, Chen J, Feng S, Wang D, et al. Advances in beidou navigation satellite system (bds) and satellite navigation augmentation technologies. *Satellite Navigation* (2020) 1:1–23. doi:10.1186/s43020-020-00010-2

61. Salamin MA, Das S, Madhav B, Lakrit S, Roy A, Zugari A. A miniaturized printed uwb antenna with dual notching for x-band and aeronautical radio navigation applications. *Telkomnika* (2020) 18:2668–77. doi:10.12928/telkomnika.v18i6.16119

62. Xu Y, Guan G, Song Q, Jiang C, Wang L. Heuristic and random search algorithm in optimization of route planning for Robot's geomagnetic navigation. *Comput Commun* (2020) 154:12–7. doi:10.1016/j.comcom.2020.02.043

63. Ning X, Gui M, Fang J, Dai G, Liu Y. A novel differential Doppler measurement-aided autonomous celestial navigation method for spacecraft during approach phase. *IEEE Trans Aerosp Electron Syst* (2017) 53:587–97. doi:10.1109/taes.2017.2651558

64. Barbour N, Schmidt G. Inertial sensor technology trends. *IEEE Sensors J* (2001) 1:332–9. doi:10.1109/7361.983473

65. Gadola M, Buffoli A, Sansa M, Berthelot A, Robert P, Langfelder G. 1.3 mm2 nav-grade NEMS-based gyroscope. *J Microelectromech Syst* (2021) 30:513–20. doi:10.1109/jmems.2021.3088940

66. Zhang Y, Yu S, Guo K, Sun J, Wu X, Xiao D. A high-performance rate-integrating hemispherical resonant gyros with 0.00753°/h bias instability. In: 2021 IEEE International Symposium on Inertial Sensors and Systems (INERTIAL). Kailua-Kona, HI, USA: IEEE (2021). p. 1–4.

67. Jeanroy A, Grosset G, Goudon JC, Delhaye F. Hrg by sagem from laboratory to mass production. In: 2016 IEEE International Symposium on Inertial Sensors and Systems. Laguna Beach, CA, USA: IEEE (2016). p. 1–4. doi:10.1109/isiss.2016.7435530

68. Sanders S, Strandjord L, Mead D. Fiber optic gyro technology trends-a honeywell perspective. In: 2002 15th Optical Fiber Sensors Conference Technical Digest. OFS 2002 (Cat. No. 02EX533). Portland, OR, USA: IEEE (2002). p. 5–8.

69. Sanders GA, Sanders SJ, Strandjord LK, Qiu T, Wu J, Smiciklas M, et al. Fiber optic gyro development at honeywell. *Fiber optic sensors Appl XIII (Spie)* (2016) 9852:37–50. doi:10.1117/12.2228893

70. Kitching J, Knappe S, Donley EA. Atomic sensors - a review. *IEEE Sensors J* (2011) 11:1749–58. doi:10.1109/jsen.2011.2157679

71. Degen CL, Reinhard F, Cappellaro P. Quantum sensing. *Rev Mod Phys* (2017) 89:035002. doi:10.1103/revmodphys.89.035002

72. Kitching J. Chip-scale atomic devices. *Appl Phys Rev* (2018) 5:031302. doi:10.1063/1.5026238

73. Fang J, Qin J. Advances in atomic gyroscopes: A view from inertial navigation applications. *Sensors* (2012) 12:6331–46. doi:10.3390/s120506331

74. Cheuk L. *Progress towards a k-rb-21ne comagnetometer* (2010).

75. Renon G, Zahzam N, Bidel Y, Bresson A, Nacher PJ. A nuclear-electronic spin gyro-comagnetometer. In: *APS division of atomic, molecular and optical physics meeting abstracts* (2014). p. M6–002.

76. Jiang L, Quan W, Liang Y, Liu J, Duan L, Fang J. Effects of pump laser power density on the hybrid optically pumped comagnetometer for rotation sensing. *Opt Express* (2019) 27:27420–30. doi:10.1364/oe.27.027420

77. Jiang L, Quan W, Liu F, Fan W, Xing L, Duan L, et al. Closed-loop control of compensation point in the k- rb- 21 ne comagnetometer. *Phys Rev Appl* (2019) 12:024017. doi:10.1103/physrevapplied.12.024017

78. Huang J, Wang Z, Fan W, Xing L, Zhang W, Duan L, et al. Analysis and suppression of the polarization error for the optical rotation detection system in an atomic comagnetometer. *Opt Express* (2020) 28:35748–60. doi:10.1364/oe.406073

79. Jiang L, Quan W, Li R, Fan W, Liu F, Qin J, et al. A parametrically modulated dual-axis atomic spin gyroscope. *Appl Phys Lett* (2018) 112:054103. doi:10.1063/1.5018015

80. Fan W, Quan W, Liu F, Xing L, Liu G. Suppression of the bias error induced by magnetic noise in a spin-exchange relaxation-free gyroscope. *IEEE Sensors J* (2019) 19:9712–21. doi:10.1109/jsen.2019.2929505

81. Fan W, Quan W, Liu F, Duan L, Liu G. Low drift nuclear spin gyroscope with probe light intensity error suppression*. *Chin Phys. B* (2019) 28:110701. doi:10.1088/1674-1056/ab44a5

82. Buchner M, Höfler K, Henne B, Ney V, Ney A. Tutorial: Basic principles, limits of detection, and pitfalls of highly sensitive squid magnetometry for nanomagnetism and spintronics. *J Appl Phys* (2018) 124:161101. doi:10.1063/1.5045299

83. Okada Y, Hämäläinen M, Pratt K, Mascarenas A, Miller P, Han M, et al. Babymeg: A whole-head pediatric magnetoencephalography system for human brain development research. *Rev Scientific Instr* (2016) 87:094301. doi:10.1063/1.4962020

84. Boto E, Holmes N, Leggett J, Roberts G, Shah V, Meyer SS, et al. Moving magnetoencephalography towards real-world applications with a wearable system. *Nature* (2018) 555:657–61. doi:10.1038/nature26147

85. Kamada K, Ito Y, Kobayashi T. Human mcg measurements with a high-sensitivity potassium atomic magnetometer. *Physiol Meas* (2012) 33:1063–71. doi:10.1088/0967-3334/33/6/1063

86. Wyllie R, Kauer M, Smetana G, Wakai R, Walker T. Magnetocardiography with a modular spin-exchange relaxation-free atomic magnetometer array. *Phys Med Biol* (2012) 57:2619–32. doi:10.1088/0031-9155/57/9/2619

87. Sulai I, DeLand Z, Bulatowicz M, Wahl C, Wakai R, Walker T. Characterizing atomic magnetic gradiometers for fetal magnetocardiography. *Rev Scientific Instr* (2019) 90:085003. doi:10.1063/1.5091007

88. Zhang SL, Cao N. A synthetic optically pumped gradiometer for magnetocardiography measurements*. *Chin Phys. B* (2020) 29:040702. doi:10.1088/1674-1056/ab7801

89. Yang Y, Xu M, Liang A, Yin Y, Ma X, Gao Y, et al. A new wearable multichannel magnetocardiogram system with a serf atomic magnetometer array. *Scientific Rep* (2021) 11:1–11. doi:10.1038/s41598-021-84971-7

90. Zhang G, Zeng H, Tan G, Lin Q. An integrated high-sensitivity vcsel-based spin-exchange relaxation-free magnetometer with optical rotation detection. *IEEE Sensors J* (2022) 22:7700–8. doi:10.1109/jsen.2022.3156814

91. Xia H, Ben-Amar Baranga A, Hoffman D, Romalis M. Magnetoencephalography with an atomic magnetometer. *Appl Phys Lett* (2006) 89:211104. doi:10.1063/1.2392722

92. Johnson C, Schwindt PD, Weisend M. Magnetoencephalography with a two-color pump-probe, fiber-coupled atomic magnetometer. *Appl Phys Lett* (2010) 97:243703. doi:10.1063/1.3522648

93. Johnson CN, Schwindt P, Weisend M. Multi-sensor magnetoencephalography with atomic magnetometers. *Phys Med Biol* (2013) 58:6065–77. doi:10.1088/0031-9155/58/17/6065

94. Shah VK, Wakai RT. A compact, high performance atomic magnetometer for biomedical applications. *Phys Med Biol* (2013) 58:8153–61. doi:10.1088/0031-9155/58/22/8153

95. Kim K, Begus S, Xia H, Lee SK, Jazbinsek V, Trontelj Z, et al. multi-channel atomic magnetometer for magnetoencephalography: A configuration study. *NeuroImage* (2014) 89:143–51. doi:10.1016/j.neuroimage.2013.10.040

96. Sheng J, Wan S, Sun Y, Dou R, Guo Y, Wei K, et al. Magnetoencephalography with a cs-based high-sensitivity compact atomic magnetometer. *Rev Scientific Instr* (2017) 88:094304. doi:10.1063/1.5001730

97. Du PC, Li JJ, Yang SJ, Wang XT, Zhuo Y, Wang F, et al. Observing the steady-state visual evoked potentials with a compact quad-channel spin exchange relaxation-free magnetometer. *Chin Phys. B* (2019) 28:040702. doi:10.1088/1674-1056/28/4/040702

98. Zhang G, Huang S, Xu F, Hu Z, Lin Q. Multi-channel spin exchange relaxation free magnetometer towards two-dimensional vector magnetoencephalography. *Opt Express* (2019) 27:597–607. doi:10.1364/oe.27.000597

99. Borna A, Carter TR, Goldberg JD, Colombo AP, Jau YY, Berry C, et al. A 20-channel magnetoencephalography system based on optically pumped magnetometers. *Phys Med Biol* (2017) 62:8909–23. doi:10.1088/1361-6560/aa93d1

100. Borna A, Carter TR, Colombo AP, Jau YY, McKay J, Weisend M, et al. Non-invasive functional-brain-imaging with an opm-based magnetoencephalography system. *Plos one* (2020) 15:e0227684. doi:10.1371/journal.pone.0227684

101. Zhang R, Xiao W, Ding Y, Feng Y, Peng X, Shen L, et al. Recording brain activities in unshielded Earth's field with optically pumped atomic magnetometers. *Sci Adv* (2020) 6:eaba8792. doi:10.1126/sciadv.aba8792

102. Hill RM, Boto E, Rea M, Holmes N, Leggett J, Coles LA, et al. Multi-channel whole-head opm-meg: Helmet design and a comparison with a conventional system. *NeuroImage* (2020) 219:116995. doi:10.1016/j.neuroimage.2020.116995

103. Rea M, Holmes N, Hill RM, Boto E, Leggett J, Edwards LJ, et al. Precision magnetic field modelling and control for wearable magnetoencephalography. *NeuroImage* (2021) 241:118401. doi:10.1016/j.neuroimage.2021.118401

104. Vivekananda U, Mellor S, Tierney TM, Holmes N, Boto E, Leggett J, et al. Optically pumped magnetoencephalography in epilepsy. *Ann Clin Transl Neurol* (2020) 7:397–401. doi:10.1002/acn3.50995

105. Mellor S, Tierney TM, O'Neill GC, Alexander N, Seymour RA, Holmes N, et al. Magnetic field mapping and correction for moving op-meg. *IEEE Trans Biomed Eng* (2021) 69:528–36.

106. Seymour RA, Alexander N, Mellor S, O'Neill GC, Tierney TM, Barnes GR, et al. Using opms to measure neural activity in standing, mobile participants. *NeuroImage* (2021) 244:118604. doi:10.1016/j.neuroimage.2021.118604

107. Tierney TM, Levy A, Barry DN, Meyer SS, Shigihara Y, Everatt M, et al. Mouth magnetoencephalography: A unique perspective on the human hippocampus. *NeuroImage* (2021) 225:117443. doi:10.1016/j.neuroimage.2020.117443

108. Cao F, An N, Xu W, Wang W, Yang Y, Xiang M, et al. Co-registration comparison of on-scalp magnetoencephalography and magnetic resonance imaging. *Front Neurosci* (2021) 15:706785. doi:10.3389/fnins.2021.706785

109. An N, Cao F, Li W, Wang W, Xu W, Wang C, et al. Multiple source detection based on spatial clustering and its applications on wearable opm-meg. *IEEE Trans Biomed Eng* (2022) 2022:3161830. doi:10.1109/tbme.2022.3161830

110. An N, Cao F, Li W, Wang W, Xu W, Wang C, et al. Imaging somatosensory cortex responses measured by opm-meg: Variational free energy-based spatial smoothing estimation approach. *Iscience* (2022) 25:103752. doi:10.1016/j.isci.2022.103752

111. Brookes MJ, Boto E, Rea M, Shah V, Osborne J, Holmes N, et al. Theoretical advantages of a triaxial optically pumped magnetometer magnetoencephalography system. *NeuroImage* (2021) 236:118025. doi:10.1016/j.neuroimage.2021.118025

112. Boto E, Shah V, Hill RM, Rhodes N, Osborne J, Doyle C, et al. Triaxial detection of the neuromagnetic field using optically-pumped magnetometry: Feasibility and application in children. *NeuroImage* (2022) 252:119027. doi:10.1016/j.neuroimage.2022.119027

113. Tang J, Zhai Y, Cao L, Zhang Y, Li L, Zhao B, et al. High-sensitivity operation of a single-beam atomic magnetometer for three-axis magnetic field measurement. *Opt Express* (2021) 29:15641–52. doi:10.1364/oe.425851

114. Yan Y, Lu J, Zhang S, Lu F, Yin K, Wang K, et al. Three-axis closed-loop optically pumped magnetometer operated in the serf regime. *Opt Express* (2022) 30:18300–9. doi:10.1364/oe.458367

115. Boto E, Seedat ZA, Holmes N, Leggett J, Hill RM, Roberts G, et al. Wearable neuroimaging: Combining and contrasting magnetoencephalography and electroencephalography. *NeuroImage* (2019) 201:116099. doi:10.1016/j.neuroimage.2019.116099

116. Hill RM, Boto E, Holmes N, Hartley C, Seedat ZA, Leggett J, et al. A tool for functional brain imaging with lifespan compliance. *Nat Commun* (2019) 10:1–11. doi:10.1038/s41467-019-12486-x